卫星干扰源定位技术
专题材料汇编

四川·成都·393信箱104号

2003年1月

卫星干扰源定位技术专题材料汇编

目 录

卢炳忠　平良子 收集整理

INTERNATIONAL JOURNAL OF SATELLITE COMMUNICATIONS, VOL. 15, 155–183 (1997)

INTERFERENCE LOCALIZATION FOR EUTELSAT SATELLITES–THE FIRST EUROPEAN TRANSMITTER LOCATION SYSTEM

D. P. HAWORTH[1,*], N. G. SMITH[1], R. BARDELLI[2] AND T. CLEMENT[2]
[1]*DERA, Defford, Worcestershire WR8 9DU, UK*
[2]*EUTELSAT, 70 rue Balard, F - 75502, Paris Cedex 15, France*

SUMMARY

In order to combat the problem of interference on EUTELSAT satellites, a study was let to the Defence Evaluation and Research Agency (DERA), Defford, UK. This study investigated transmitter location using two-satellite techniques; time difference of arrival (TDOA) and frequency difference of arrival (FDOA). The study produced predictions that interference could be located to tens of km using pairs of EUTELSAT II satellites in north/south stationkept orbits. If a satellite in an inclined orbit, such as a EUTELSAT I, was used, the interference could be located an order of magnitude more accurately. The dominant cause of location error was found to be the satellite ephemeris accuracy in predicting velocity. The theoretical findings were backed up with a successful measurement campaign which targeted both test signals from a known location and operational traffic.

Int. J. Satell. Commun., **15**, 155–183 (1997)

No. of Figures: 31 No. of Tables: 11 No. of References: 14

KEY WORDS: transmitter location systems; TDOA; FDOA; EUTELSAT; interference

1. INTRODUCTION

Events such as 'Captain Midnight's' capture of the Home Box Office's Galaxy II transponder in 1986[1] has raised awareness to the threat of unwanted signals on commercial communications satellites. These signals can range from the deliberate unauthorized use by 'Captain Midnight', through to the accidental interference caused by a malfunctioning very small aperture terminal (VSAT).

The clear trend towards proliferation of satellite ground terminals, and the increasing congestion of the geostationary arc, has increased activity in the detection and location of unauthorized access of satellite communications channels.[2,3]

For a number of years staff at the Defence Evaluation and Research Agency (DERA), Defford, UK, have been pursuing a programme to investigate, both practically and theoretically, the detection and subsequent location of unwanted signals accessing communications satellite channels serving military needs.

Work started in late 1982 with an investigation into the potential for interference on channels designed for mobile communications at UHF(~300 MHz) and followed on from unpublished work performed in the USA.[4,5] Initial locations were demonstrated using frequency difference of arrival techniques (FDOA) on continuous wave (CW) signals in 1983 and 1984, and using both FDOA and time difference of arrival (TDOA) techniques on modulated signals in 1985. Further work was carried out at SHF(~8 GHz) between 1986–1990, to investigate the potential of locating unauthorized access of satellite channels. Starting in 1987, DERA has supported and collaborated with the US Naval Space Command on the location of interference of UHF communications satellite channels.[6–9]

In 1993, DERA became aware of interest from the European Telecommunications Satellite Organization (EUTELSAT) in its transmitter location system (TLS). Subsequently, EUTELSAT let a study to DERA aimed at identifying the most suitable technique for localizing sources of satellite interference, evaluating its expected performance in the EUTELSAT environment and demonstrating the actual performance of a system implementing the selected technique.[10] Following this study, DERA now provides a commercial transmitter location service to EUTELSAT.

In Section 2, the technique of location using pairs of satellites is presented. In Section 3, results of a measurement campaign to demonstrate the technique in the EUTELSAT environment are presented. In Section 4, possible improvements to the transmitter location system are discussed and Section 5 concludes.

2. TECHNIQUE

The technique used in DERA's TLS relies on the measurement of TDOA and/or FDOA of interfering

Published with the permission of the controller of Her Majesty's Stationery Office.
*Correspondence to: D.P. Haworth, DERA, Defford, Worcestershire WR8 9DU, UK

CCC 0737–2884/97/040155–30$17.50

Accepted 1 September 1997

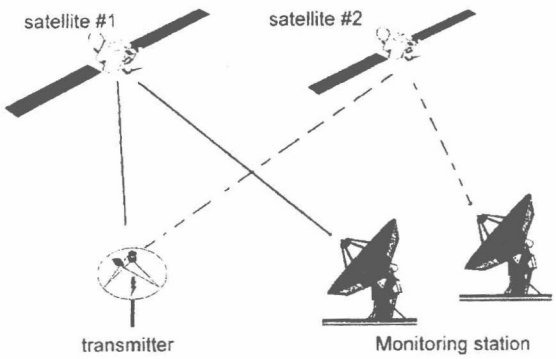

Figure 1. Multiple satellite transmitter location configuration

signals propagating through both the communications satellite that is interfered and adjacent satellites in the geostationary arc (Figure 1). The different path lengths via the two satellites produce the TDOA and the different residual movements of the satellites, relative to the ground, produce the FDOA at the monitoring station. The TDOA/FDOA technique is well known and can be traced at least as far back as a technique to locate celestial sources using long baseline inteferometry.[11] The accuracy of the technique has been discussed by Chestnut.[12]

A problem arises in practice in that the overspill from commercial satellite terminals into adjacent satellites is very weak and hard to detect by conventional measurement techniques. However, correlation techniques enable the weak signal to be detected and the TDOA and FDOA can therefore be measured.[13] Signals from the two paths are correlated together with different time and frequency offsets until a peak response in the correlation power is obtained. The time and frequency offsets of the peak can be related to the TDOA and FDOA. Once the TDOA and FDOA have been determined, these can be combined with knowledge of the satellites' position and velocity at the time of observation to derive lines of position (LOP) on the earth. These LOP intersect at the location of the radio frequence (RF) interference.

If FDOA- or TDOA-only measurements are possible (e.g. for an RF interferer that is not modulated, FDOA-only measurements can be made) then time-separated measurements of TDOA or FDOA can be combined to yield a location for the RF interference. With this technique, TDOA or FDOA measurements are made at times usually separated by several hours. Each measurement can be used to generate a LOP on the earth and the elapsed time between measurements enables the earth/satellite geometry to change sufficiently to enable separately identifiable LOPs which intersect at the signal source location. The technique is considered in more detail below.

A signal from an interfering transmitter is illuminating the main (interfered) satellite. Due to the finite size of the transmitter antenna, there are sidelobes of varying levels in the direction of adjacent satellites in the sky. If these satellites have transponders at the transmitter frequency, they will also relay a weak version of the transmitter signal to the ground. The signals from the two satellites can be observed at a suitable monitoring station. The signals via the two satellite paths arrive at slightly different times due to the different path lengths, and at different frequencies due to a combination of the satellites' translation oscillators and the Doppler shift induced by the satellite motion. These different times and frequencies can be used to infer the location of the transmitter. The challenge is to:

(a) detect the very weak signals in the adjacent satellite channel–often in the presence of an access on the adjacent satellite;
(b) measure the delay and frequency shift;
(c) convert these measurements into an accurate location.

These challenges are considered in the following sections.

2.1. *Detection*

The detection of very weak signals is achieved through correlation techniques. A generalized correlation technique that uses both frequency and time offsets is cross ambiguity function (CAF) processing.

The CAF is defined by[13]:

$$A(\tau,\nu) = \int_{-T/2}^{T/2} s_1(t)s_2^*(t+\tau)e^{-i2\pi\nu t}dt \qquad (1)$$

where s_1 and s_2 are the complex envelopes of the two signals that contain a common component, τ and ν are the time lag and frequency offset parameters, respectively, to be searched simultaneously for the values that cause $|A(\tau,\nu)|$ to be a maximum, and finally T is the duration of the correlation. The post-correlation signal-to-noise ratio (SNR) is given by:

$$\mathrm{SNR} = \frac{2\,BT\,\mathrm{snr}^2}{k[1+\mathrm{snr}(1+1/k)]} \qquad (2)$$

where snr is the input SNR in the main satellite

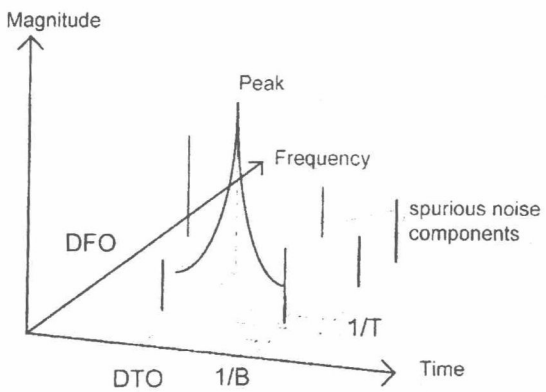

Figure 2. CAF magnitude and spurious noise components

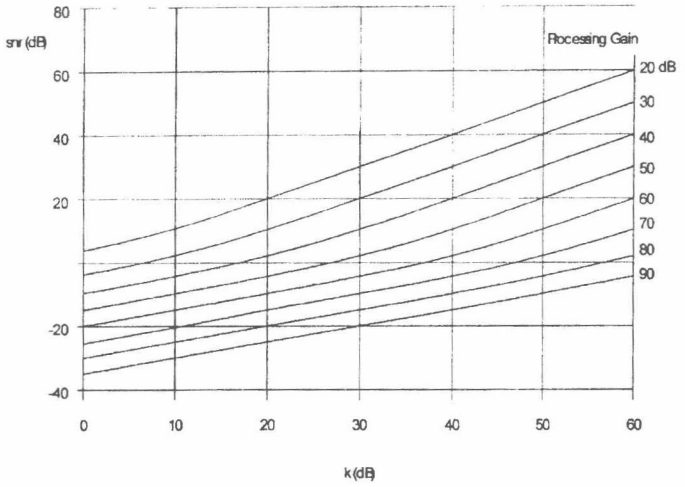

Figure 3. Relationship between main channel SNR (snr) and discrimination between main and overspill channels with PG as a parameter. The post correlation SNR is taken to be 20 dB

channel (as measured in the downlink receiver), B is the channel noise bandwidth (assumed identical in both channels), T is the integration time, and finally, k is the 'overspill factor' defined by:

$$k = \text{snr(main channel)}/\text{snr(overspill channel)}\,. \tag{3}$$

The term $2BT$ is called the processing gain (PG). It can be shown for signals taken at the Nyquist rate that there are $2BT$ independent samples available in a time length T, hence

$$2\,BT = N \tag{4}$$

where N is the number of sample points per channel. The number of sample points per channel determines the processing power of a practical TLS.

In order to unambiguously identify the correlation peak, the peak has to significantly exceed the background noise. Figure 2 schematically shows the magnitude of the CAF correlation in the time-frequency domain. The existence of spurious correlations due to noise, requires a post-correlation SNR of about 20 dB.

Equations (1), (2) and (3) show that the ability to perform a correlation depends on the received SNR of the downlink from the communication satellite, subject to interference, as well as the relative downlink SNRs in the communication and overspill satellite channels. Thus factor k is a rough measure of the directivity of the emitter antenna. However, the performance of the ground station monitoring the satellite downlinks is also important, as is the sensitivity of the individual satellite channels. The PG is a measure of the performance of equipment used to carry out signal processing. The relationship between the various terms is shown in Figure 3.

Because of the wide variety of signal levels, antenna types and waveform types in satellite communications systems and the possibility of outside interference, it is difficult to assess whether in general the signal will be detectable in an adjacent satellite channel. Apart from the radiation characteristics of the interfering transmitter antenna and the transmit power, the impact of having other signals in both the interfered and adjacent satellite channels needs to be considered (including intermodulation and cross-polar signals). In the application of Equation (2), these signals may be treated as a simple noise contribution.

By using knowledge of the environment, the relationship between antenna performance and the SNR as received at the two ground terminals, it is possible to infer the antenna size that would be detectable for a given satellite angular separation, or conversely, for a given antenna size, what the maximum possible angular separation where the signal could be detected in the second satellite channel.

Figure 4 shows a set of examples of antenna sidelobe envelopes for likely antenna sizes at Ku band. The envelopes are drawn from International Radio Consultative Committee (ITU) (CCIR) recommendations.[14]

To take a specific example, consider a TLS with a PG of 60 dB. With reference to Figure 1, the interfering signal is assumed to have a 10 dB SNR as measured at the monitoring station looking at satellite #1. It is further assumed that the sensitivity of the adjacent satellite #2 channel is identical to the satellite #1 channel. Examination of Figure 3 shows that a discrimination factor k of 50 dB could be accommodated and still yield a reliable correlation. From Figure 4, the detection could be achieved with satellites up to 6° apart for a transmitter antenna diameter of 11 m and with satellites up to 20° apart for an antenna diameter of 3 m.

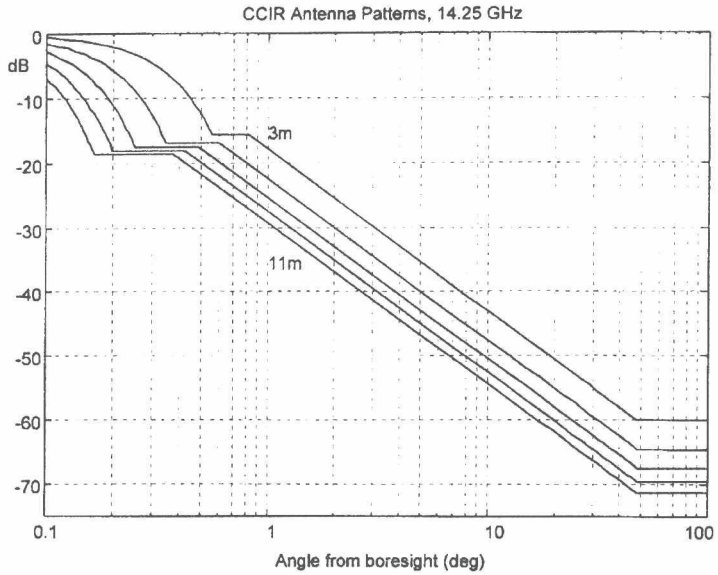

Figure 4. CCIR sidelobe envelope antenna patterns at 14·25 GHz

2.2. *Parameter estimation*

Once a signal has been detected, the inherent accuracy achievable in differential time offset (DTO) and differential frequency offset (DFO) measurements is described by the following equations which represent fundamental limits of parameter estimation formulas[13]:

$$\sigma_\tau = \frac{1}{B_u\sqrt{\mathrm{SNR}}}\,;\ \sigma_\nu = \frac{1}{T_u\sqrt{\mathrm{SNR}}} \tag{5}$$

where σ_τ is the root mean square (rms) DTO uncertainty and σ_ν is the rms DFO uncertainty. Finally, SNR is the post-correlation SNR as defined in Equation (2) and the terms B_u and T_u are the rms bandwidth and duration of the signal, respectively, and are defined by[13]:

$$T_u = 2\pi\sqrt{\frac{\int_{-T/2}^{T/2} t^2|u(t)|^2dt}{\int_{-T/2}^{T/2}|u(t)|^2dt}}\,;$$

$$B_u = 2\pi\sqrt{\frac{\int_{-\infty}^{\infty} f^2G_u(f)df}{\int_{-\infty}^{\infty}G_u(f)df}} \tag{6}$$

where $u(t)$ is the time domain signal and G_u is the power spectral density of the signal.

It can be seen from Equations (5) and (6) that, for an assumed value of SNR, the accuracy of DTO estimation depends directly on the rms bandwidth of the signal and the accuracy of the DFO estimation depends directly on the rms duration of the signal.

It is possible to process the signals in a different way depending on whether DTO or DFO is being estimated in order to maximize measurement accuracy. Thus, to estimate DTO, signals are processed in the maximum available bandwidth. To estimate DFO, signals are processed in the maximum available time. Given the constraint of a fixed PG, such as would be available from a typical, practical TLS, this would mean samples for DTO processing are taken in the widest available bandwidth and samples for DFO processing are of narrow bandwidth and a relatively long duration.

Figure 5a,b illustrates how the DTO error is dependent on symbol rate for a typical digital signal and how the DFO error is dependent on analysis bandwidth. Note, for the DFO error the available PG determines the time duration of the sample for a given analysis bandwidth.

Apart from the fundamental limits of parameter estimation from a signal, there are other error contributions which must be taken into account. These contributions include measurement equipment, propagation and satellite ephemeris. These errors and their impact reduction are considered further in the following section.

2.3. *Error contributions and reduction of their impact*

Figure 6 shows the contributions to TDOA and FDOA observation errors. Clearly the effects which are most important are those which perturb timing and frequency. Propagation effects can delay the signal, satellite translation oscillator differences will directly affect the FDOA, delay differences on the satellite will directly affect TDOA, errors in satellite positions will directly affect TDOA and errors in

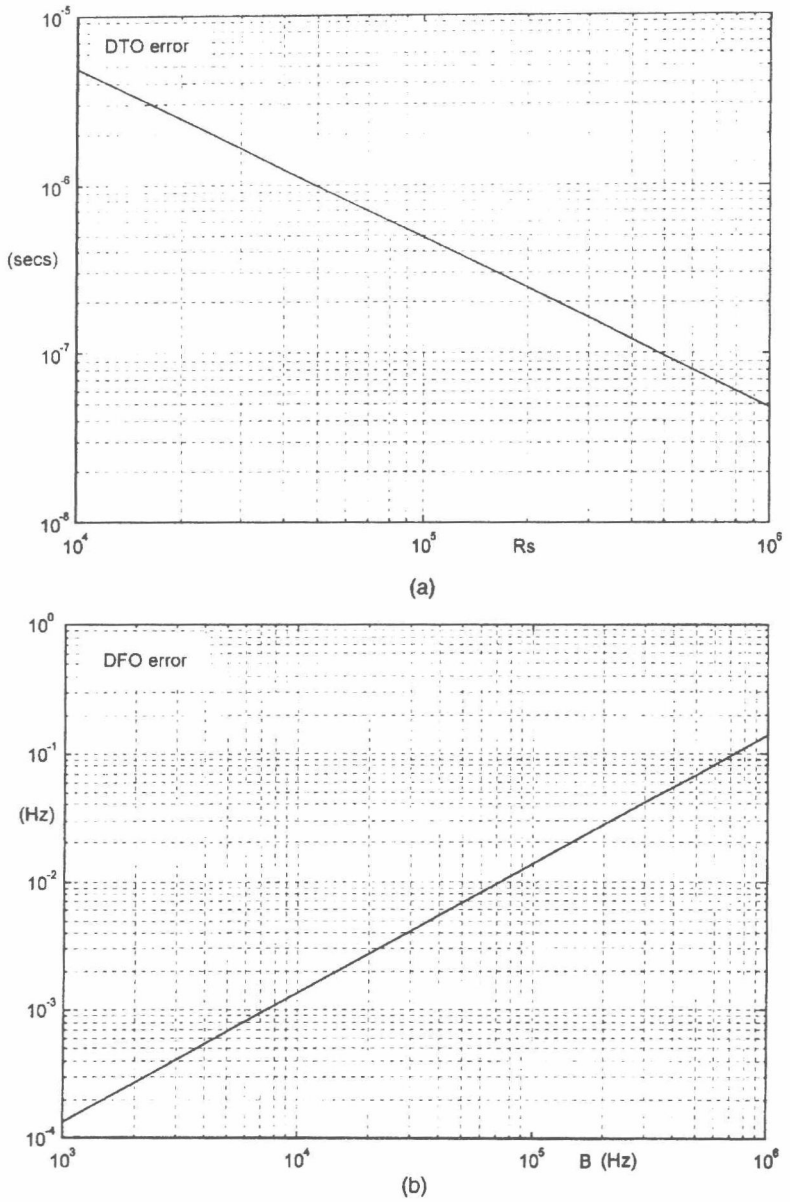

Figure 5. (a) Variation of DTO error with symbol rate for a 20 dB SNR. (b) Variation of DFO error with analysis bandwidth for a 20 dB post correlation SNR and a 60 dB processing gain

satellite velocities will directly affect FDOA. Further errors can be introduced at the monitoring station.

Figure 7 shows the use of a reference signal (heavy lines) transmitted over the satellite channels and monitored at the same time as the unknown transmitter. The reference signal has a number of specific benefits:

(a) the satellite and downlink paths (including monitoring station equipment) are common to the unknown and reference signals, so that satellite oscillator and delay errors are cancelled as well as downlink propagation effects;

(b) the reference signal originates from a point of known location (in this example the monitoring station). This enables the unknown transmitter to be located relative to the monitoring station. It can be shown that errors in satellite position and velocity produce effects on TDOA and FDOA that are common to the unknown and monitoring sites and thereby their effects are reduced.

In order to quantify these benefits, Table I summarizes the typical errors on TDOA and FDOA with and without a reference signal.

It can be seen from Table I that some effects are completely cancelled through the use of a reference and other effects are reduced by an order of magnitude or more. It can be seen in this example that, in the absence of the parameter estimation errors discussed in Section 2.2. there is a residual error in TDOA of around 0·1 μs and in FDOA of around

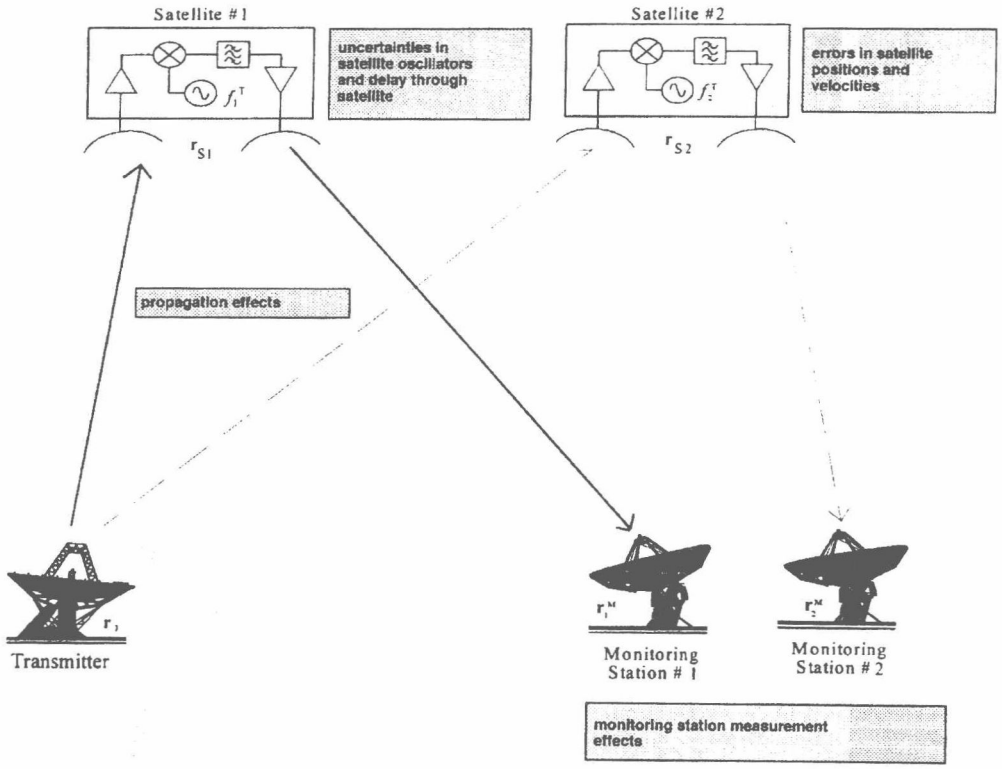

Figure 6. Contributions to TDOA and FDOA observation errors

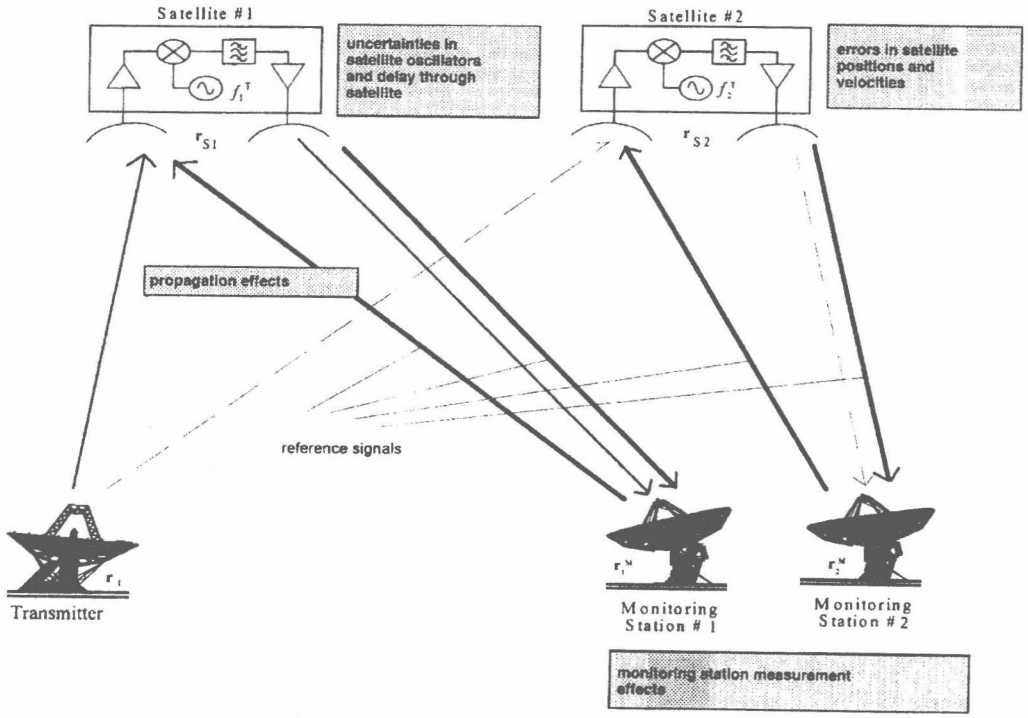

Figure 7. Use of reference signal to correct errors

Table I. Effect of reference signal on TDOA and FDOA errors

TDOA error term	Value without reference (s)	Value with reference (s)
Propagation	5×10^{-8}	2×10^{-8}
Satellite delay	1×10^{-8}	0
Satellite position	2×10^{-6}	1×10^{-7}
Monitoring station	1×10^{-7}	5×10^{-9}

FDOA errors term	Value without reference (Hz)	Value with reference (Hz)
Propagation	$<1 \times 10^{-3}$	$<1 \times 10^{-3}$
Satellite translation oscillators	10	0
Satellite velocity	2	$1{\cdot}4 \times 10^{-2}$
Monitoring station	10	0

Estimates are for adjacent Eutelsat II satellites and for unknown transmitter and reference sites around 1000 km apart.

14 mHz. Thus, even with perfect measurements of DTO and DFO there can still be a significant location error.

2.4. *Locations from observations*

In order to move from observations of TDOA and FDOA to a location of a transmitter, it is necessary to determine the positions and velocities of the satellites at the time of observation, and, from the geometry, to determine LOPs on the earth corresponding to the observed TDOA and FDOA. The intersection of the LOP give the location of the transmitter.

2.4.1. *Geometry of transmitter location.*

Figure 8 shows the basic geometry of transmitter location. A signal radiated from a source at $\mathbf{r}$ is received by two satellites at $\mathbf{r}_{S1}$ and $\mathbf{r}_{S2}$. The signal is then relayed by the satellites to a monitoring station at $\mathbf{r}_m$. Note that, unless stated otherwise, the origin of vectors is the centre of the earth.

The TDOA and FDOA are given by

$$(\mathrm{TDOA})_{21} = \frac{1}{c}\left[(l_2 + l_2^m) - (l_1 + l_1^m)\right]$$

$$= \frac{1}{c}\left(|\mathbf{r}_{S2} - \mathbf{r}| + |\mathbf{r}_{S2} - \mathbf{r}_m| - |\mathbf{r}_{S1} - \mathbf{r}| - |\mathbf{r}_{S1} - \mathbf{r}_m|\right), \quad (7)$$

$$(\mathrm{FDOA})_{21} = -\frac{f}{c}\mathbf{v}_{S2} \cdot \mathbf{u}_2(\mathbf{r}) - \frac{1}{c}(f - f_2^T)\mathbf{v}_{S2} \cdot \mathbf{u}_2(\mathbf{r}_m) + \frac{f}{c}\mathbf{v}_{S1} \cdot \mathbf{u}_1(\mathbf{r}) + \frac{1}{c}(f - f_1^T)\mathbf{v}_{S1} \cdot \mathbf{u}_1(\mathbf{r}_m), \quad (8)$$

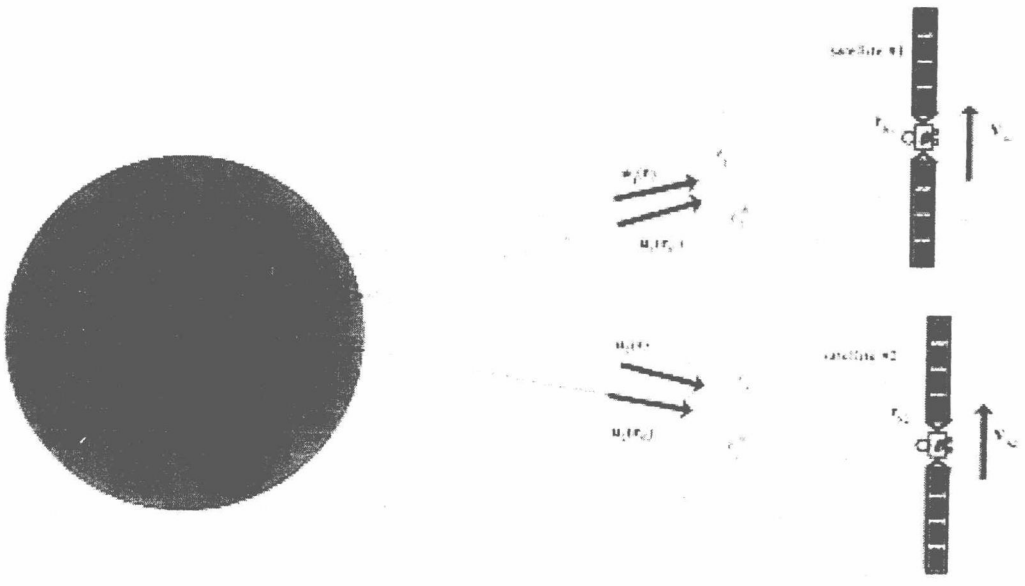

Figure 8. Geometry of transmitter location

where

$\mathbf{r}$ = position vector to source on ground,
$\mathbf{r}_m$ = position vector to monitoring station on ground,
$\mathbf{r}_{Si}$ = position vector to ith satellite ($i = 1,2$),
$\mathbf{v}_{Si}$ = velocity vector to ith satellite,
$\mathbf{u}_i$ = unit vector from point to $\mathbf{r}_{Si}$,
f = signal frequency,
f_i^T = translation oscillator frequency on ith satellite ($i = 1,2$),
c = velocity of light.

Equations (7) and (8) represent a somewhat idealized description of the TDOA and FDOA and have neglected some effects such as propagation, in order to concentrate on the geometrical factors.

The TDOA in Equation (7) comprises an uplink and downlink component. For any fixed monitoring station and fixed satellite position, the variation of TDOA due to the position of an unknown signal source will be purely on the uplink component. Likewise for the variation of FDOA. Consequently, in understanding geometrical effects, the uplink TDOA and FDOA are of prime interest. A further simplification is obtained by normalizing the operating frequency and the velocity of light, in order to use just the uplink differential slant range (DSR) and the uplink differential slant range rate (DSRR).

The uplink DSR and DSRR are given by

$$\begin{aligned} \text{DSR} = l_{21} &= c \,.\, \text{TDOA}_{\text{uplink}} \\ &= |\mathbf{r}_{S2} - \mathbf{r}| - |\mathbf{r}_{S1} - \mathbf{r}| \,, \end{aligned} \tag{9}$$

$$\begin{aligned} \text{DSRR} = v_{21} &= -\frac{c}{f} \text{FDOA}_{\text{uplink}} \\ &= \mathbf{v}_{S2} \,.\, \mathbf{u}_2 - \mathbf{v}_{S1} \,.\, \mathbf{u}_1 \,. \end{aligned} \tag{10}$$

For a typical satellite geometry, LOPs can be drawn on the earth which satisfy particular observations of TDOA and FDOA and consequently result in a constant DSR and DSRR. An example of accurate DSR and DSRR LOPs are given in Figure 9.

For small eccentricities and inclinations such as experienced on commercial communications satellites, the difference in satellite position vectors is nearly in the equatorial plane and orthogonal to the line from the satellites to the centre of the earth. Consequently, DSR LOPs look like straight lines in the perspective of Figure 9. Furthermore, they will remain virtually time independent.

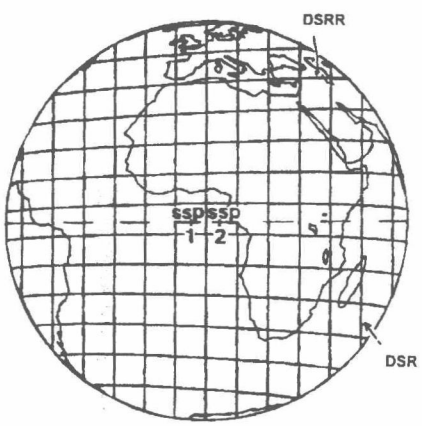

Figure 9. Lines of position (LOP)

In contrast, the DSRR LOPs will be dependent on the velocity difference of the two satellites. This velocity difference will be strongly time dependent and will have components both in the direction of the earth and orthogonal to this direction. Often the DSRR LOP will have similar form to the DSR LOP but orientated in a different direction. In extreme circumstances, the DSRR LOP will form concentric ellipses.

2.4.2. *Relationship between errors in location and TDOA and FDOA errors.*

In order to understand the impact of errors on the location solution obtained from the intersection of DSR and DSRR LOPs, a matrix equation is derived which relates small changes in DSR and DSRR to small changes in position. Specifically:

$$\begin{bmatrix} dl_{21} \\ dv_{21} \end{bmatrix} = \begin{bmatrix} a_{11} & a_{12} \\ a_{21} & a_{22} \end{bmatrix} \begin{bmatrix} dE \\ dN \end{bmatrix} \equiv d\underline{\mathbf{k}}_{21} = \underline{\mathbf{A}}_{21} \,.\, \underline{\mathbf{d}}_{21} \,,$$

$$\text{and } \underline{\mathbf{d}}_{21} = \underline{\mathbf{A}}_{21}^{-1} \,.\, d\underline{\mathbf{k}}_{21} \tag{11}$$

where;

$$\begin{aligned} a_{11} &= \underline{\nabla} l_{21} \,.\, \mathbf{e}_E \,, \; a_{12} = \underline{\nabla} l_{21} \,.\, \mathbf{e}_N \,, \\ a_{21} &= \underline{\nabla} v_{21} \,.\, \mathbf{e}_E \,, \; a_{22} = \underline{\nabla} v_{21} \,.\, \mathbf{e}_N \,, \end{aligned} \tag{12}$$

$\mathbf{e}_E$ and $\mathbf{e}_N$ are unit vectors pointing locally east and north, respectively, at point $\mathbf{r}$ and dE and dN are infinitesimal changes in the east and north directions, respectively.

In order to treat random measurement errors, the covariance matrix $\underline{\mathbf{C}}$ can be defined where

$$\underline{\mathbf{C}} = \langle \underline{\mathbf{d}}_{21} \underline{\mathbf{d}}_{21}^T \rangle \equiv [c_{ij}] \,, \text{ and}$$

$$c_{11} = \sigma_E^2 = \frac{1}{D^2} [a_{12}^2 \sigma_v^2 + a_{22}^2 \sigma_l^2]$$

$$c_{12} = \rho_{EN}^2 = -\frac{1}{D^2} [\sigma_l^2 a_{21} a_{22} + \sigma_v^2 a_{11} a_{12}]$$

$$c_{21} = c_{12}$$

$$c_{22} = \sigma_N^2 = \frac{1}{D^2} [a_{11}^2 \sigma_v^2 + a_{21}^2 \sigma_l^2] \tag{13}$$

where σ_l is the rms DSR uncertainty and σ_v is the rms DSRR uncertainty. Also σ_E is the rms east-west location uncertainty, σ_N is the rms north-south location uncertainty and ρ_{EN} denotes the fact that, in general, the east-west and north-south uncer-

tainties will be correlated. The rms components describe an error ellipse within which there is about a 50 per cent probability of finding the location of the transmitter. This error ellipse is shown schematically in Figure 10. Additionally:

$$D = |a_{11}a_{22} - a_{12}a_{21}| = (\nabla l_{21} \wedge \nabla v_{21}) \,.\, \mathbf{e}_r \,,$$

$$\text{and } \mathbf{e}_r = \frac{\mathbf{r}}{r} \,. \tag{14}$$

Finally, a total rms position uncertainty σ can be defined:

$$\sigma \equiv \frac{1}{D} \sqrt{\sigma_l^2(a_{22}^2 + a_{21}^2) + \sigma_v^2(a_{12}^2 + a_{11}^2)} \,. \tag{15}$$

Thus, in summary, it is possible to define a rms location error (in km) and relate this to the DSR and DSRR errors and thence to the TDOA and FDOA errors. Equation (15) can be further simplified and the notation rationalized. It can be shown that

$$\sigma = \frac{1}{|\sin \varphi|} \sqrt{\frac{\sigma_l^2}{L_t^2} + \frac{\sigma_v^2}{V_t^2}} \tag{16}$$

where

σ_l = rms DSR error = $c \times$ TDOA error,
σ_v = rms DSRR error = $c \times$ FDOA error/f,
L_t = magnitude of the component of the DSR gradient in the azimuth plane at the point $\mathbf{r}$ on the earth,
V_t = magnitude of the component of the DSRR gradient in the azimuth plane,
φ = angle between components of DSR and DSRR gradient in the azimuth plane = angle between LOPs on the earth's surface at point $\mathbf{r}$.

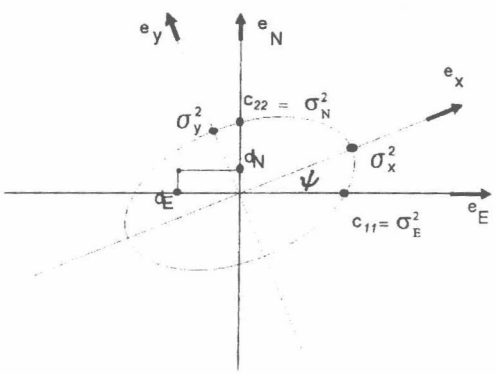

Figure 10. Showing the components of the location error ellipse. The principal axis variances and inclination of the ellipse are related to the **C** matrix elements as follows

$$\sigma_x^2 = \frac{c_{11} + c_{22}}{2} + \frac{c_{12}}{\sin 2\psi} \,;\; \sigma_y^2 = \frac{c_{11} + c_{22}}{2} - \frac{c_{12}}{\sin 2\psi} \,;$$

$$\tan 2\psi = \frac{2c_{12}}{c_{11} - c_{22}} \,.$$

The DSR and DSRR gradients are given (with reference to Figure 8) by

$$\nabla l_{21}(\mathbf{r}) = -(\mathbf{u}_2 - \mathbf{u}_1) \,, \tag{17}$$

$$\nabla v_{21}(\mathbf{r}) = \left\{ \frac{1}{l_2} [\mathbf{v}_{S2} - (\mathbf{v}_{S2} \,.\, \mathbf{u}_2)\mathbf{u}_2] - \frac{1}{l_1} [\mathbf{v}_{S1} - (\mathbf{v}_{S1} \,.\, \mathbf{u}_1)\mathbf{u}_1] \right\} , \tag{18}$$

$$\nabla = \mathbf{e}_x \frac{\partial}{\partial_x} + \mathbf{e}_y \frac{\partial}{\partial_y} + \mathbf{e}_z \frac{\partial}{\partial_z} \,. \tag{19}$$

where $\mathbf{e}_x$, $\mathbf{e}_y$, and $\mathbf{e}_z$ are unit vectors along the x, y and z orthogonal axes.

An important aspect of Equation (16) is that the contributions of TDOA and FDOA errors are combined in a root sum square manner. Thus, there is a contribution to the location error from the TDOA error which can be separately analyzed from the contribution to the location error from the FDOA error. Consequently, an analysis can be performed with only TDOA errors for which a specific location error in km/μs can be derived and an analysis can be performed with only the FDOA error for which a specific location error in km/mHz can be derived. These specific location errors can be combined in a root sum square manner once the actual measurement errors are determined. Thus, the measurement specific aspects can be separated from the purely geometrical aspects allowing waveform independent analysis of the geometric aspects.

2.4.3. *Spatial and temporal variation of location error.*

Section 2.4.2. has given the basic formulae that relates location error to the DSR and DSRR errors through the earth/satellite geometry. How this location error varies with position and time is clearly of interest and this is considered later in this section.

2.4.3.1. *Spatial variation.* It is a simple matter to determine DSR, DSRR and rms location errors (assuming DSR and DSRR errors) for a given pair of satellites at a fixed point in time and over a regular grid of points on the earth. From this grid, LOPs and typical location errors can be derived. Figure 11a,b shows the LOPs and specimen rms location error for a combination of EUTELSAT IIF2 and IIF4 satellites which are adjacent in their orbits at 10 and 7° east, respectively.

Equation (16) shows that $\sigma \rightarrow \infty$ if any of L_t, V_t or φ are zero. For L_t or V_t to be zero, the modulus of the gradients themselves could be zero or the gradients are normal to the surface of the earth. For φ to be zero, the LOPs must run parallel. In Figure 11a,b, it can be seen that there is a line

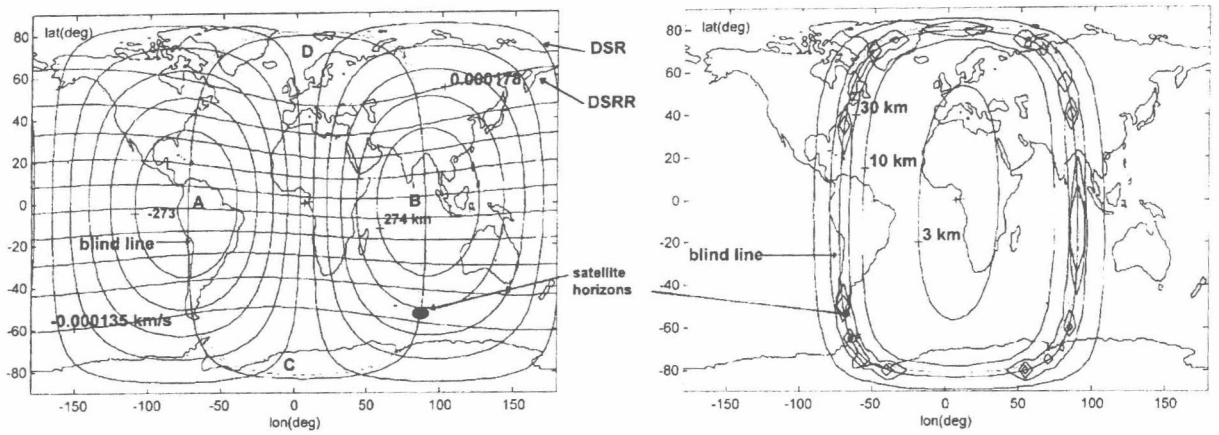

Figure 11. (a) DSR and DSRR contours of the Eutelsat IIF2/IIF4 conbination at 0500 h on 28 January 1994. (b) Rms location error with assumed TDOA and FDOA observation errors of 0·5 μs and 1 mHz respectively

along which the rms location error tends to infinity, this line is termed the 'blind line' indicating that location is not possible. For the illustration in Figure 11a,b, the blind line is close to the horizon of the satellites, thus ensuring effective location over most of the visible earth. The LOPs run parallel close to the horizon because of the curvature of the earth. Furthermore, it can be shown that L_t goes to zero at points A and B and V_t goes to zero at points C and D.

A typical pair of satellites in near geostationary orbit (i.e. with a small but significant inclination of the orbit to the equator) has the DSR gradient along an east-west line at the mean sub-satellite point. The DSRR gradient typically points along the earth's rotation axis. At the mean sub-satellite point, the DSRR and DSR gradients are entirely in the azimuth plane and are orthogonal. For a given DSR and DSRR error, the rms location error is minimized at the sub-satellite point. The situation has been illustrated in Figure 11a. In Figure 11a the component of DSRR gradient in the azimuth plane goes to zero around the North and South Poles. Likewise, the azimuth component of the DSR gradient goes to zero around the Indian Ocean and Peru. Also the DSR and DSRR LOPs run parallel along the blind line which, in this figure, lies very close to the satellite horizons.

In the simplified case where the DSR gradient is exactly along the east-west direction and the DSRR gradient is exactly along the north-south direction at the mean sub-satellite point, it is found that

$$L_t = L\sqrt{1 - \cos^2 \beta \sin^2 \alpha}\ ;\ V_t = V \cos \beta\ ;$$

$$\sin \varphi = \frac{\cos \alpha}{\sqrt{1 - \cos^2 \beta \sin^2 \alpha}} \qquad (20)$$

where α is the longitude of **r**, relative to the mean sub-satellite point, and β is the latitude of **r**.

It can be seen that, for a given geometry of satellites at a fixed instant in time, the rms location error increases with distance away from the mean sub-satellite point.

As the location of **r** moves north from the mean sub-satellite point, the angle φ remains at around 90°. Furthermore, the component of the DSR gradient in the azimuth plane remains constant (at $\alpha = 0$). However, the component of the DSRR gradient in the azimuth plane reduces as cos β, thereby increasing the contribution of the DSRR error to the overall rms location error.

As the location of **r** moves east from the mean sub-satellite point, the angle φ again remains around 90°. Furthermore, the component of the DSRR gradient in the azimuth plane remains constant. However, the component of the DSR gradient in the azimuth plane reduces as cos α, thereby increasing the contribution of the DSR error to the overall rms location error.

2.4.3.2. *Temporal variation.* Figure 12 shows the rms location error at Paris as a function of time. Twice per day the rms location error tends to infinity. The precise causes of the large location error at these times will be clarified in this section.

To examine temporal variation, it is appropriate to take a single point **r** on the earth and to evaluate how the location error at this point behaves over time. From Equation (16), the temporal behaviour will depend on the variation with time of the DSR and DSRR gradients projected onto the azimuth plane. The DSR gradient is dependent directly on the angular separation between satellites as viewed from point **r**. For low inclination angles (~0·1°), the angular separation between satellites will stay nearly constant with time. For higher inclination angles (~1°) there will be a significant variation in angular separation, but varying about some mean non-zero value.

The DSRR gradient projected into the azimuth plane is determined by the rate of change of the projected differential sky trace (PDST). In order to explain this, it is appropriate to view the PDST at

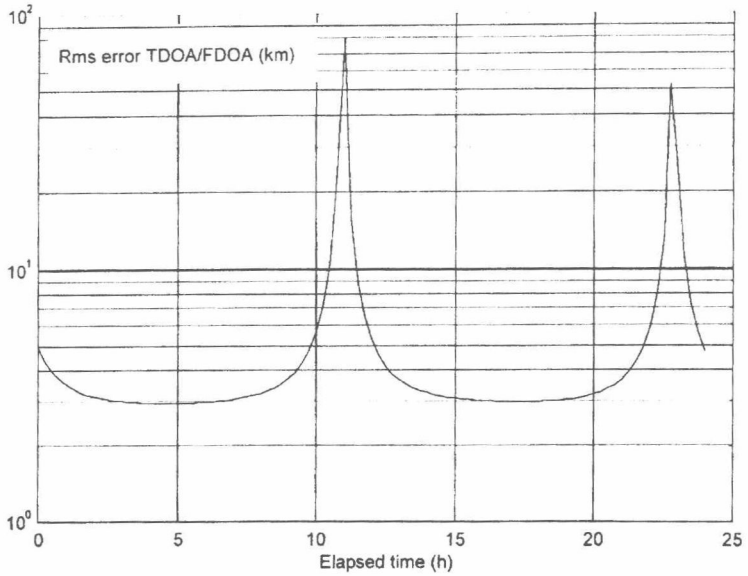

Figure 12. Rms location error at Paris for the TDOA and FDOA observation errors of 0·5 μs and 1 mHz

point **r** to the satellites as shown in Figure 13. In general, as both satellites are moving, and it is the separation between satellites that is of interest for the DSR gradient, it is appropriate to view the motion of the second satellite relative to the first. As a large net drift of the position of one satellite relative to the second is unlikely, the motion of the second satellite relative to the first will tend to form a closed figure. This situation is shown in Figure 14. A sufficient condition for a 'blind' time, when location is not possible, is for the determinant given in Equation (14) to go to zero. This condition occurs when the projected DSRR gradient is zero or is aligned along the DSR gradient projected into the azimuth plane. The blind times can be inferred by drawing lines from the origin, tangent to the PDST. At the tangent points, the projected DSR and DSRR gradients run parallel. It will be possible to draw at least two lines tangent to the PDST and therefore there will be at least two blind times for the DSR/DSRR measurement.

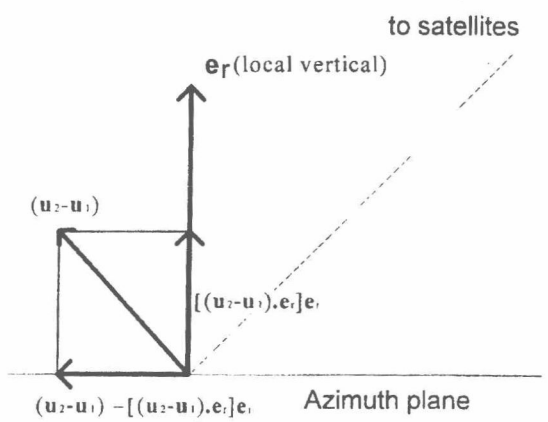

Figure 13. Showing the projection process for the PDST

It can be seen from Figure 14, that the approximate duration of blind times depends on the behaviour of the PDST. For example, if the PDST oval is orientated with its longer axis along the direction of the projected DSR gradients, then the duration of blind times will be longer than if the PDST oval is orientated with its shorter axis along the direction of the projected DSR gradients. The detailed behaviour will depend on the geometry of specific cases.

The magnitude of the DSRR gradient is indicated by the magnitude of the variation of the DSR gradient with time. The direction of the DSRR gradient is indicated by the tangent to the PDST and the magnitude is indicated by the length of the PDST change per hour.

From the temporal behaviour, it is possible to select a poor time of day and look at the spatial behaviour at the poor time. This behaviour can then be contrasted against the behaviour at a good time of day.

Figure 12 has shown the typical rms error evolution at Paris for the EUTELSAT IIF2 and IIF4 satellite combination predicted for 28 January 1994. The equivalent PDST is shown in Figure 15.

It can be seen from the PDST that there is a linear drift of one satellite relative to the other. Nevertheless, the turning points in the PDST, will closely identify the blind times to around 11:00 and 23:00 h. Figure 15 clearly ties in well with Figure 12 in predicting the blind times. From Figure 12, the times of day of the largest location error at Paris are around 11:00 and 23:00 h.

Finally Figure 16a,b gives the LOP and spatial variation of rms location error at 11:00 h and shows the blind line running through Paris.

2.4.4. *Impact of ephemeris and other errors.*

Ephemeris and other errors and their reduction through the use of reference signals were considered

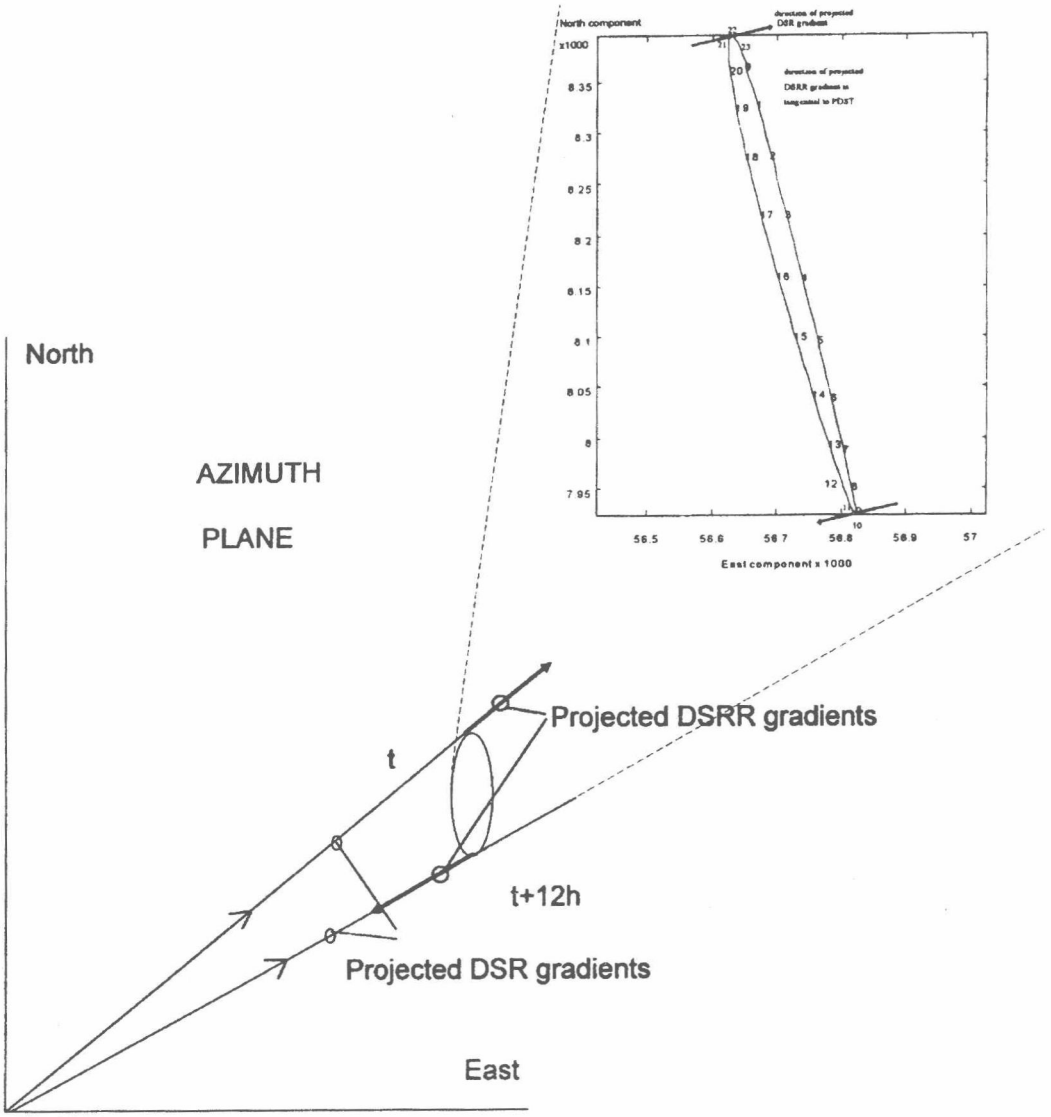

Figure 14. PDST

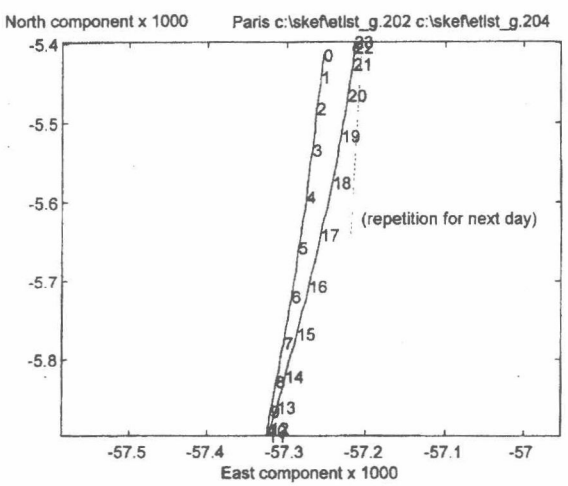

Figure 15. PDST for Eutelsat IIF2/IIF4 combination for 28 January 1994

in Section 2.3. Table I summarized typical equivalent errors due to propagation, satellite ephemeris and other errors. These errors are dominated by satellite ephemeris errors. For the satellite and reference site combination considered, residual TDOA and FDOA errors of around 0·1 μs and 14 mHz were achieved. It has been found that the minimum specific location error (as discussed in Section 2.4.2.) for the EUTELSAT IIF2/IIF4 combination was around 5 km/μs and 1 km/mHz. Thus the minimum location error possible for the residual errors is around $\sqrt{(0{\cdot}5^2 + 14^2)}$ km = 14 km.

It can be seen that the minimum achievable error is dominated by the ephemeris error impact on FDOA which, in turn, is due to errors in the measurement and prediction of satellite velocities. This fact is not surprising when it is considered that FDOA can be measured on a signal to around 1 mHz. At 14 GHz, 1 mHz corresponds to a velocity of around 0·02 mm/s. This velocity error is generally

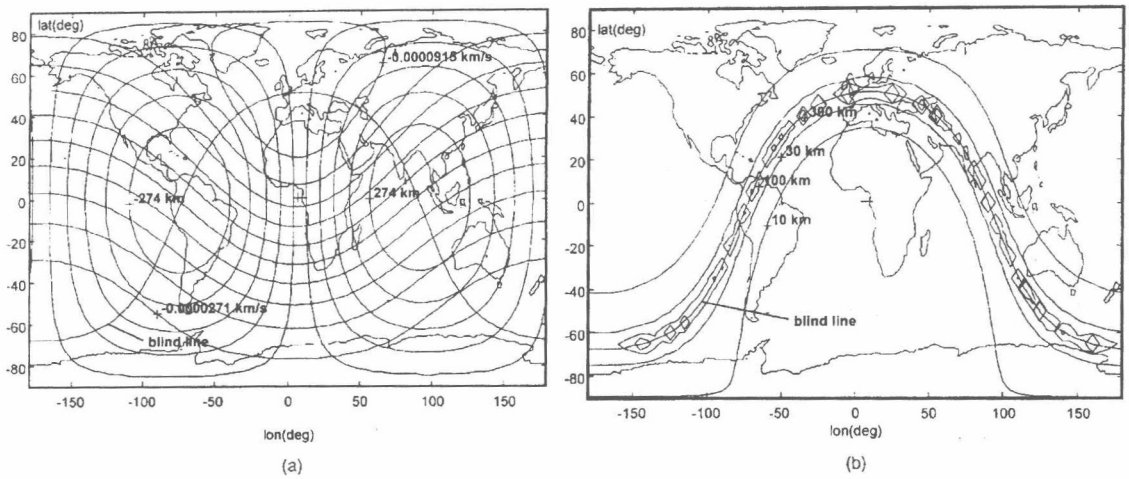

Figure 16. (a) Showing the DSR and DSRR LOP for the Eutelsat IIF2/IIF4 combination. Note that, at this time (11:00) the blind line is running through Paris. (b) Rms location error for Eutelsat IIF2/IIF4 combination at worst time of day for Paris location. TDOA error is 0·5 μs and FDOA error is 1 mHz

much less than achieved through normal ephemeris measurement and prediction techniques, and special techniques are therefore necessary to exploit the full potential of the FDOA measurement.

Two techniques can be used to refine ephemeris information. The first is to perform locations on sources at known locations to derive corrections to the satellite ephemerides. The second is to use the initial location to find closer sources to the unknown signal to use as references.

The first technique has the advantage that, once the refinement has been performed, the refined ephemeris is generally applicable until the next satellite stationkeeping manoeuvre. However, a disadvantage is that the measurements required to improve ephemeris need to be performed over an extended time (typically 24 h).

The second technique has the advantage that it can be performed quickly. The main disadvantage is that there needs to be a source of known location that is in the vicinity of the unknown source.

In concluding this section it should be noted that ephemeris improvement is the subject of ongoing research.

2.4.5. *Observations based on TDOA only or FDOA only.*

In general circumstances, it is preferable to make combined TDOA/FDOA observations. In some circumstances however, it may be necessary to measure only the DTO or only the DFO of the interfering signal. An example of a DTO-only measurement would be a wideband TV signal where the power density in a narrow band could be small, or a sweeping interferer where the occupancy in a narrowband was very limited. An example of a DFO-only measurement would be on a CW signal where there was no modulation from which to determine timing information.

Equation (16) has given the rms location error for combined TDOA/FDOA observations. It is simple to extend this formulation to time separated measurements.

TDOA-only

For TDOA-only observations, Equation (16) can be extrapolated to:

$$\sigma = \frac{1}{|\sin \varphi|} \sqrt{\frac{\sigma_t^2(t_1)}{L_t^2(t_1)} + \frac{\sigma_t^2(t_2)}{L_t^2(t_2)}} \qquad (21)$$

FDOA-only

For FDOA-only observations, Equation (16) can be extrapolated to:

$$\sigma = \frac{1}{|\sin \varphi|} \sqrt{\frac{\sigma_v^2(t_1)}{V_t^2(t_1)} + \frac{\sigma_v^2(t_2)}{V_t^2(t_2)}} \qquad (22)$$

For satellites with a low inclination angle of their orbital plane to the equator compared to their angular separation, the DSR gradient is relatively time independent. Furthermore, the error in DSR is usually relatively time independent. With these assumptions, Equation (21) can be simplified further to:

$$\sigma = \frac{\sigma_t \sqrt{2}}{L_t |\sin \varphi|} \qquad (23)$$

For TDOA-only observations with the simplifying assumption of a constant DSR gradient, the location performance is governed by the angle between the LOPS at the separate times of observation. For wideband TV signals, a DTO error of 10 ns is achievable. However, in Table I the error introduced through ephemeris uncertainty is of the order of 120 ns and so this error will dominate the TDOA observation. For FDOA-only observations, the

ephemeris uncertainty will introduce an error of typically 18 mHz and this is likely to dominate the DFO measurement error. For the combination of EUTELSAT IIF1 and IIF2 satellites, the results are shown in Figure 17a,b.

The use of time-separated measurements brings an additional degree of freedom which is the separation time between measurements. Figure 18a,b shows the variation of rms location error with a separation time between observations for TDOA and FDOA measurements, respectively. Again the example is a pair of EUTELSAT II satellites separated by 3° in their orbits. It can be seen that there is a clear dependence with time separation for the TDOA observations, but not a clear dependence for the FDOA observations. However, care is necessary in generalizing the interpretation of these plots due to their dependence on the detailed orbital parameters of the satellites involved.

2.5. *DERA's transmitter location system*

DERA's TLS is located at Defford, Worcestershire, UK. The system is designed to work with satellites which operate over any frequency band for which there are available ground stations.

Figure 19 shows the configuration of the DERA TLS. Two ground stations are connected at an intermediate frequency (IF) to four receivers. One receiver each is used to receive the unknown and reference signals from each satellite. The receivers act as signal conditioners converting the high IF to a much lower IF and filtering the signals in the required bandwidth. After conditioning, signals are

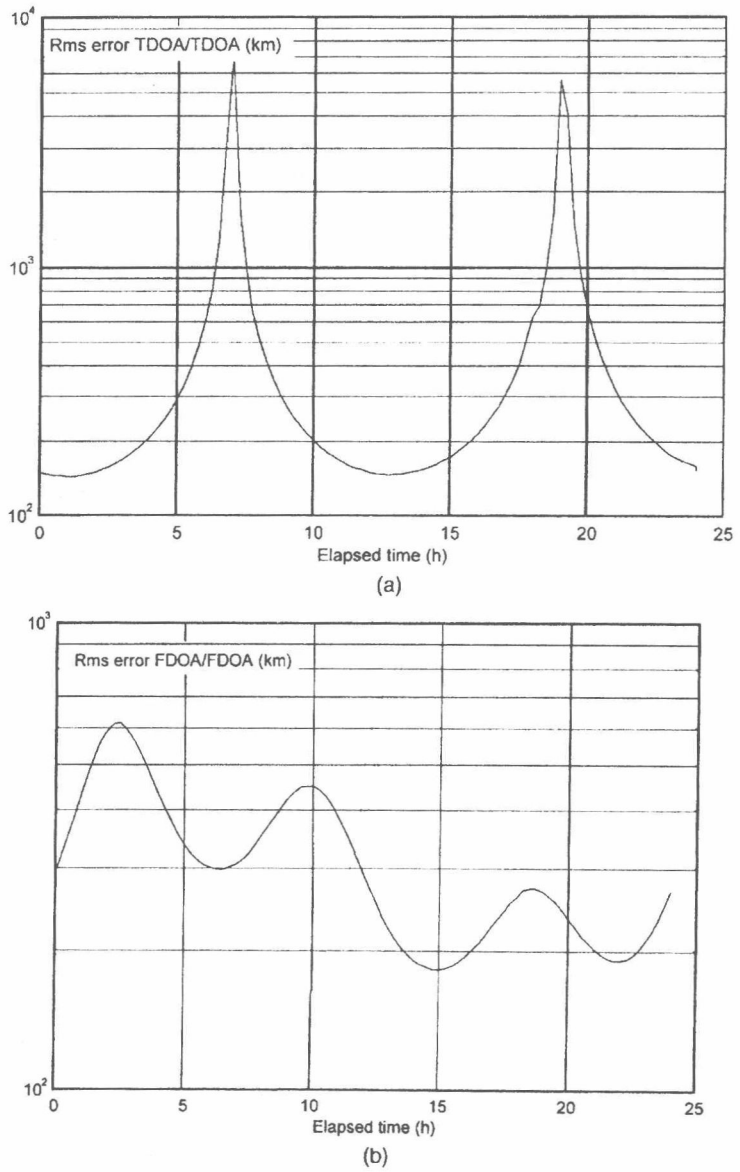

Figure 17. (a) Example of location error for time-separated TDOA observations. Time separation is 6 h. (b) Example of location error for time-separated FDOA observations. Time separation 6 h

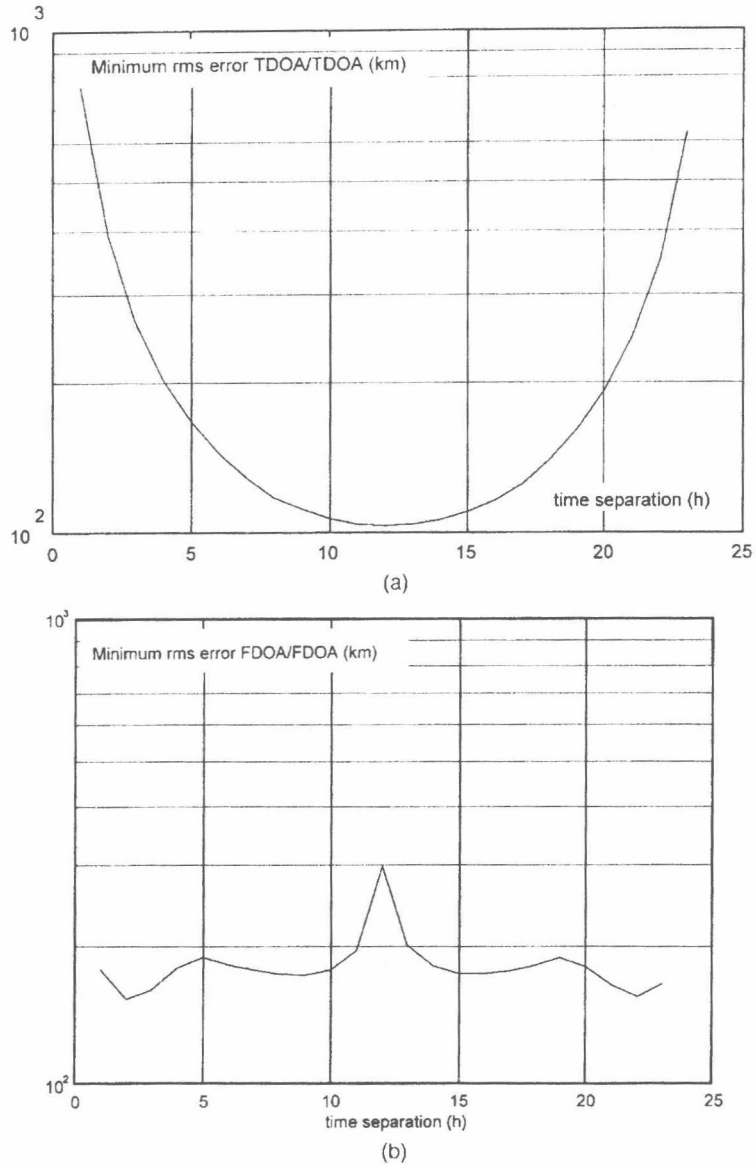

Figure 18. (a) Variation of minimum rms error with TDOA/TDOA time separation. (b) Variation of minimum rms error with FDOA/FDOA time separation

digitized and stored in memory, prior to being read into a host computer and stored on filestore. Timing integrity is maintained in absolute terms through the use of a global positioning system/very low frequency timing signal (GPS/MSF) timing receiver.

The use of the reference signal is an important feature of the measurement system. Typically, ground stations utilize downconverter units to translate the received RF signal to an IF. The IF is usually a standard frequency such as 140 MHz or 700 MHz. In the TLS any degradation added by the downconverter units is common to both the unknown and reference signals and can be subsequently removed. The DERA TLS is able to interface with the IF outputs of ground stations operating at any RF, provided the reference and unknown signals pass through the same RF and downconverter path at each ground station.

Once unknown and reference signal paths diverge, considerable care is needed to maintain timing, frequency and phase integrity of the unknown and reference signals from each ground station. For example, Rx_{1u} and Rx_{1r} typically need to have local oscillators driven by a common reference signal and ADC_{1u} and ADC_{1r} typically need to be clocked and triggered from a common source.

The major practical consideration which may cause a deviation from theoretically expected performance is mismatching the receiver bandwidth to the signal of interest. Most commercially available receivers have a limited selection of bandwidths. If these bandwidths do not match the signal of interest, then some degradation in performance will result. If the receiver bandwidth is less than the signal bandwidth, the maximum possible input SNR will be achieved and the detection performance will be